Available online at www.sciencedirect.com

ScienceDirect

Ceramics International 40 (2014) 2221–2227

CERAMICS INTERNATIONAL

www.elsevier.com/locate/ceramint

The use of a diatomite–kaolin composite coating to design the pore characteristics of a sintered diatomite membrane

Jang-Hoon Ha*, Eunji Oh, In-Hyuck Song

Powder and Ceramics Division, Korea Institute of Materials Science, 797 Changwondaero, Seongsan-gu, Changwon, Gyeongnam 642-831, Republic of Korea

Received 22 June 2013; received in revised form 18 July 2013; accepted 29 July 2013
Available online 3 August 2013

Abstract

Porous ceramic membranes have lately attracted great interest due to their outstanding thermal and chemical stability. In this paper, we report the results of our efforts to determine whether we could prepare a diatomite–kaolin composite coating to be deposited over a sintered diatomite support layer that could reduce the largest pore size of the sintered diatomite membrane while retaining an acceptable level of permeability. We determined under what conditions such a composite coating over a support layer could be prepared without the generation of micro-cracks during drying and sintering. The pore characteristics of the sintered diatomite membranes were studied by scanning electron microscopy and capillary flow porosimetry.

Keywords: A. Sintering; Porous materials; Microstructure

1. Introduction

Porous ceramics have recently become the focus of great interest [1] as researchers seek to exploit their unique properties (e.g., high wear resistance [2], low density [3], low thermal conductivity [4–6], and a low dielectric constant [7]). Notably, membranes [8–12] are among the most feasible applications of porous ceramics. The driving force for the development of porous ceramic membranes is mainly the need for membranes with greater thermal and chemical stability because most polymeric membranes cannot withstand operating temperatures above 200 °C or exposure to organic solvents such as benzene and toluene [13].

It is generally believed that the most important features of a porous ceramic membrane are its permeation and separation properties. Therefore, precisely controlling pore characteristics (e.g., size of the largest pores) while retaining an acceptable level of permeability is very important. One challenge associated with the application of ceramic membranes is determining how to control, tailor, and characterize pores, and various ceramic membrane pore shapes have been illustrated in detail [14,15]. Different approaches that afford control over microstructural features (of separation (coating) and intermediate and support layers) and ultimately determine the permeation properties of porous ceramic membranes have been assessed.

Much research has been dedicated to the study of materials commonly used for ceramic membranes (i.e., γ-Al_2O_3 [11,16], α-Al_2O_3 [10,17], TiO_2 [18,19], ZrO_2 [20], and SiO_2 [21]) and composites of these materials [22,23], but there have been only a few studies on materials that are already porous, such as diatomite, a sedimentary rock formed from the rigid, siliceous cell walls of ancient diatoms [24–26].

Previously, we reported on two of three possible approaches for fabricating a sintered diatomite membrane, which allowed for control over membrane characteristics (e.g., largest pore size and mechanical strength) while retaining an acceptable level of permeability.

The aim of the first approach is to enhance the permeability of the sintered diatomite support (DS) layers beyond that which could be achieved by controlling the sintering temperature. To this end, spherical macro-pores were induced in the sintered diatomite support layer by incorporating a sacrificial polymer template as a pore former [27]. Although the permeability of the sintered DS layers was significantly enhanced, their largest pore sizes fluctuated due to macro-pores or micro-cracks generated during pyrolysis.

*Corresponding author. Tel.: +82 55 280 3350; fax: +82 55 280 3392.
E-mail addresses: hjhoon@kims.re.kr, hjhoon@gmail.com (J.-H. Ha).

0272-8842/$ - see front matter © 2013 Elsevier Ltd and Techna Group S.r.l. All rights reserved.
http://dx.doi.org/10.1016/j.ceramint.2013.07.140

The fluctuation of the largest pore sizes was suppressed by introducing a diatomite coating. However, with this approach, there is no way to reduce the largest pore size beyond the largest pore sizes observed in a natural diatomite matrix because the coating and support layers are prepared from the same material. Therefore, the main focus was on preparing a sintered DS layer with the highest degree of permeability while retaining the largest pore size.

In the second approach, to decrease the largest pore size of the sintered DS layer even further, kaolin was added to form a sintered diatomite–kaolin composite support (DKCS) layer [28]. There are two reasons for adopting kaolin. First, it is compatible with diatomite because kaolin consists mostly of kaolinite ($Al_2Si_2O_5(OH)_4$). Its composition is similar to diatomite [29], which is mainly composed of silica (SiO_2) with small amounts of alumina (Al_2O_3). Second, the particle size of kaolin is smaller than that of diatomite. When more than a certain amount of kaolin is added, pore channels in the diatomite matrix are clogged by kaolin particles, reducing the permeability and the largest pore size simultaneously. The mechanical strength of the sintered DKCS layer is significantly enhanced as the amount of added kaolin increases. However, the largest pore size decreases linearly as the amount of added kaolin increases, whereas the permeability decreases abruptly to a level that hinders its application as a porous ceramic membrane.

Third, in this study, the focus was on determining how to decrease the largest pore size of the diatomite membrane even further while leaving the permeability unchanged. Kaolin was selected to form a sintered diatomite–kaolin composite (DKC) coating. The permeability of the separation layer (in this study, the coating) over a support layer generally governs the overall permeability of a membrane. Our goal was to prepare a well-defined DKC coating that was thick enough to reduce the largest pore size effectively and thin enough not to diminish the permeability to an unacceptable level.

To these ends, several important aspects of our ultimate goals were investigated in the present study. First, we determined whether we could decrease the largest pore size of a DKC membrane, with a minimal loss of permeability, by adopting a diatomite-matrix cover of kaolin (0–15 wt%) created under different conditions. We also investigated whether we could overcome the difference in the degree of shrinkage of the diatomite composite coating and the diatomite support layer.

2. Material and methods

Diatomite (Celite 499, Celite Korea Co. Ltd., Korea) and kaolin (Kaolin, Sigma-Aldrich, U. S. A.) were used to prepare the diatomite–kaolin composite membranes. The average particle sizes

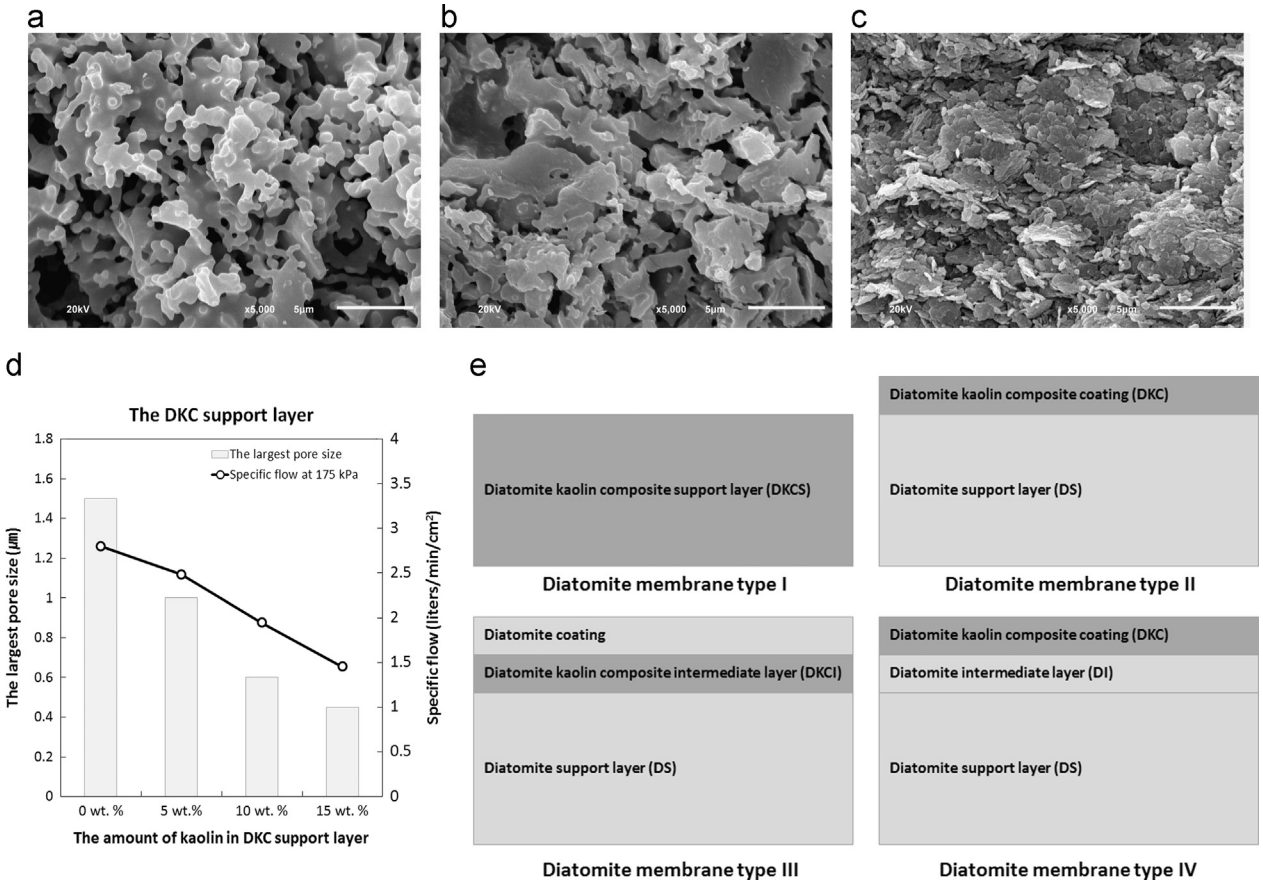

Fig. 1. Typical SEM images of diatomite–kaolin composite support layers sintered at 1200 °C for 1 h with (a) 0 wt% kaolin, (b) 50 wt% kaolin, and (c) 100 wt% kaolin. (d) The permeability and the largest pore size of the diatomite–kaolin composite support layers and (e) schematic diagrams of diatomite membranes prepared in this study (not drawn to scale).

of the starting powders were determined by a particle size analyzer (LSTM 13 320 MW, Beckman Coulter, USA). The average particle sizes of the as-received diatomite and as-received kaolin were 12.79 μm and 1.53 μm, respectively. To enhance the sintering of the diatomite particles, the average particle size of the diatomite was reduced to 7.43 μm by ball-milling. Distilled water was used as a solvent, and the slurry was ball-milled for 24 h with an alumina ball-to-powder volume ratio of 2:1. To incorporate kaolin into the diatomite matrix, diatomite particles were mixed with 0–15 wt% kaolin for 3 h by ball-milling with a ball-to-powder volume ratio of 0.5:1. With polyethylene glycol as a binder, the diatomite–kaolin composite specimens were dry-pressed at 18.7 MPa, and sintered at 1200 °C for 1 h. A dip-coating process was used to deposit a composite coating, or a composite intermediate layer, onto the diatomite support layer. For the coating process, diatomite, kaolin, distilled water, an organic binder (HS BD-25, San Nopco Korea, Korea), and an inorganic binder (AS-40, Sigma-Aldrich, USA) were mixed, dip-coated on a sintered diatomite support layer, dried at room temperature for 24 h, and then sintered at 1200 °C for 1 h.

The pore characteristics of the diatomite membranes were examined by scanning electron microscopy (JSM-5800, JEOL, Japan). The air flux was measured by capillary flow porosimetry (CFP-1200-AEL, Porous Materials Inc., U. S. A.). A sintered diatomite–kaolin composite specimen (diameter 4 cm and thickness 0.4 cm) was fitted between the O-rings in the bottom of the chamber and the bottom of the chamber insert for capillary flow porosimetry. The flux was then measured automatically by sensors while incrementing the diameter of the motorized valve and the pressure of the regulator.

3. Results and discussion

Typical scanning electron microscope (SEM) images of DKCS layers sintered at 1200 °C for 1 h with additions of 0, 50, and 100 wt% kaolin are shown in Fig. 1(a, b, and c, respectively). Although we incorporated up to 15 wt% kaolin into the diatomite support layer or diatomite coating, as shown in the high-magnification SEM image, the microstructure of the DKCS layer with 25 wt% kaolin added is similar to that of the DKCS layer with 50 wt% kaolin added. Therefore, in this study, we intended to show representative images of the microstructures of DKCS layers with 0, 50, and 100 wt% kaolin to make a clear comparison. With the addition of 50 wt % kaolin, the microstructure of the DKCS layer shows microscopic features intermediate between irregular diatomite

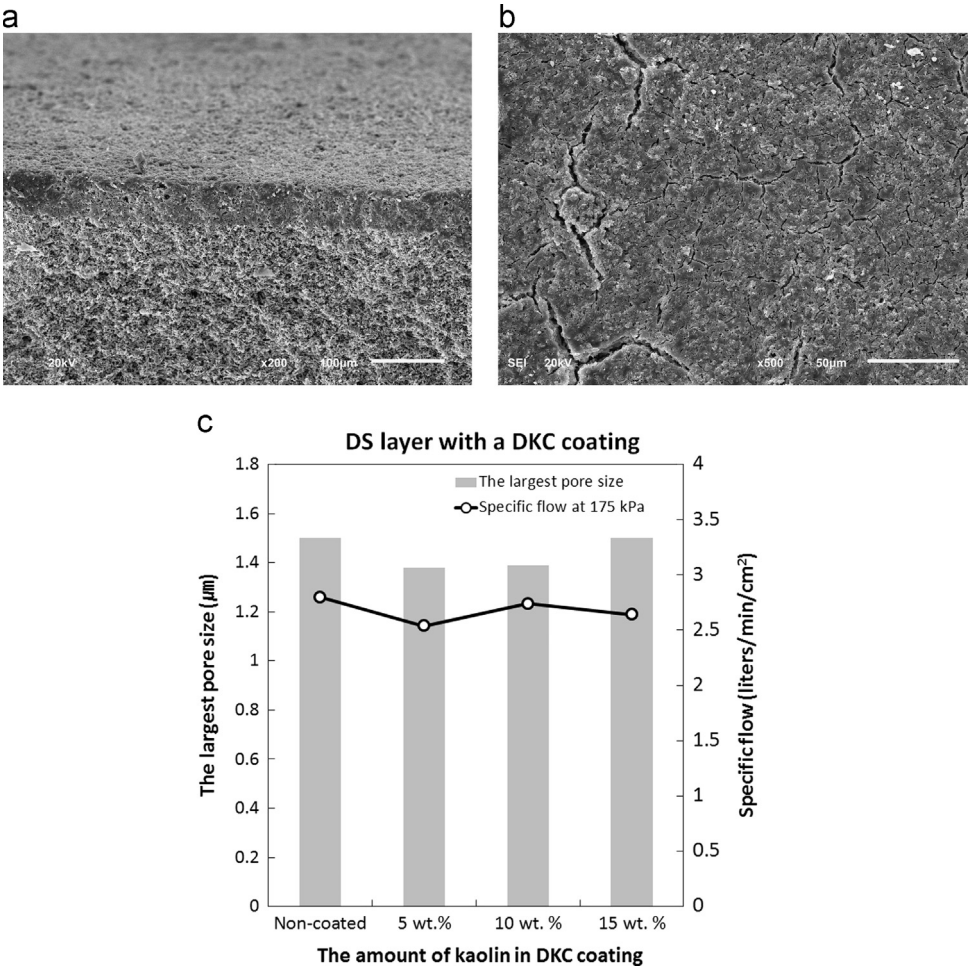

Fig. 2. (a) Cross-sectional SEM image of the diatomite–kaolin composite coating prepared with 5 wt% kaolin deposited onto a diatomite support layer and sintered at 1200 °C for 1 h, (b) a surface SEM image of the diatomite–kaolin composite coating, and (c) the permeability and largest pore size of the diatomite–kaolin composite coating deposited on the diatomite support layer.

and plate-like kaolinite. Fig. 1d shows that the permeability and largest pore size of the DKCS layer decreased as the amount of kaolin added increased. When amount of added kaolin rose above 25 wt%, even though there was no abrupt increase in density, the permeability of the DS layer decreased exponentially, as previously reported [28]. Thus, regarding the addition of kaolin as a DKCS layer (Diatomite membrane type I as shown in Fig. 1e), the enhancement in the permeability and decrease in the largest pore size of the diatomite membrane remain in a trade-off relationship. Therefore, to decrease the largest pore size of the diatomite membrane even further while retaining the desired permeability, kaolin was added to form a thin DKC coating rather than a thick support layer.

Prior to depositing a DKC coating on a DS layer (Diatomite membrane type II as shown in Fig. 1e), we were concerned as to whether the concentration of kaolin in the diatomite suspension would vary after the coating process. When a coating dries slowly on a solid support layer, the evaporation can alter the thickness profile of the coating. However, surface tension dictates that the thickness profile maintains the shape of a spherical cap so that radial flow occurs outward [30]. In contrast, in the present work, a diatomite–kaolin composite coating was rapidly dried due to the capillary force of the porous substrate used [31]. A dip-coated composite coating over a diatomite support layer was experimentally shown to dry in few seconds. The capillary flow perpendicular to the surface of the diatomite support layer induced by the pores far exceeded the radial flow parallel to the surface induced by evaporation. Therefore, even if variation of the kaolin ratio arises due to differences in particle size and density between the kaolin and diatomite before complete drying, it will not vary parallel to the surface of the support layer but perpendicular to it.

The image in Fig. 2a is a typical SEM cross-section of the DKC coating (5 wt.% kaolin) on the DS layer, after sintering at 1200 °C for 1 h. The thickness of the DKC coating was approximately 50 μm. It is difficult to find defects or delamination between the DKC coating and the DS layer in the cross-sectional SEM images (Fig. 2a), but an SEM image (Fig. 2b) of the top surface clearly reveals numerous micro-cracks on the DKC coating. Fig. 2c also supports the presence of micro-cracks in the DKC coating by showing that neither the permeability nor the largest pore size decreased significantly, regardless of the addition of the DKC coating.

To prevent the generation of micro-cracks, we considered the following critical factors of the diatomite–kaolin composite coating process. First, micro-cracks may be generated during the drying process. When a coating containing particles is dried on a support layer, evaporation of the solvent leaves the coating particles in a close-packed state. Further evaporation causes the liquid meniscus on top of the particles exert a compressive capillary force on the particles [32]. Due to the compressive stress, the coating thickness decreases linearly with time during the drying process; all of the pores are full of liquid and evaporation occurs from an upper liquid film until a critical point at which too many points of hard contact between the particles make any more plastic deformation difficult. Evaporation then begins to occur from the inside of the pores. A coating composed of rigid ceramic particles such as diatomite tends to crack during drying because the particles cannot deform to resist the formation of micro-cracks. In addition, it has been reported that these micro-cracks nucleate spontaneously during, but independent of, the drying process only when the coating reaches a 'critical cracking thickness' [33]. Because the critical cracking thickness increases with the particle size [34], a coating of fine particles is more likely to crack. In this study, the measured average particle sizes of diatomite and kaolin were 7.43 μm and 1.53 μm, respectively. Therefore, as the amount of kaolin added to the diatomite coating increased, the average particle size of the diatomite–kaolin composite coating decreased. Consequently, if the amount of kaolin in a DKC coating is too high, or its thickness is too great, the DKC coating layer is prone to crack during the drying process. However, if the amount of kaolin added is too low, the largest pore size of the coating becomes

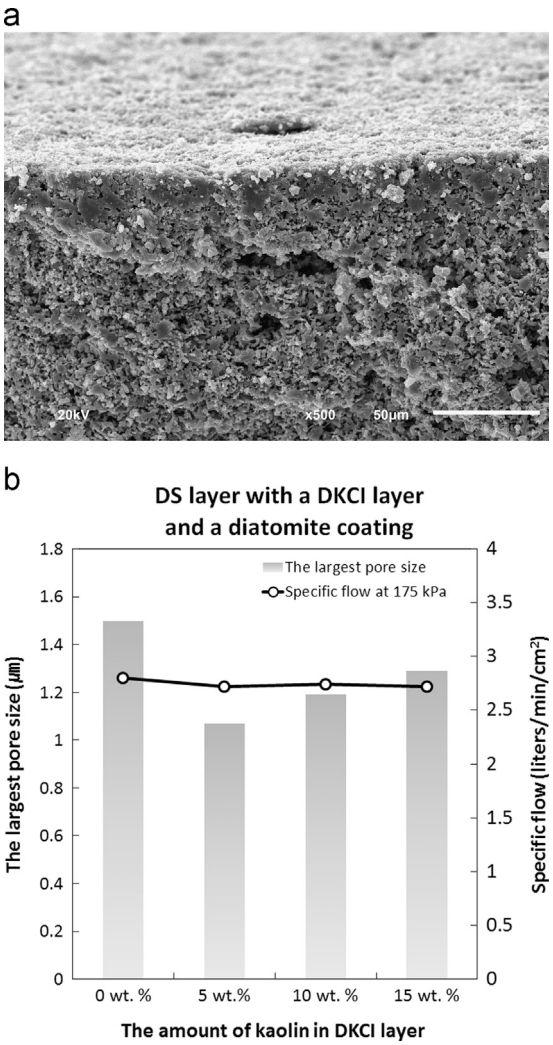

Fig. 3. (a) A cross-sectional SEM image of the diatomite coating prepared with 10 wt% kaolin deposited with a diatomite–kaolin composite intermediate layer on the diatomite support layer, and sintered at 1200 °C for 1 h. (b) The permeability and largest pore size of the diatomite–kaolin composite coating deposited over a diatomite intermediate layer on a diatomite support layer.

similar to that of the diatomite support layer, making the DKC coating useless. In this study, we were not able to obtain a DKC coating without micro-cracks, even when the amount of added kaolin was as low as 5 wt%. Furthermore, we could not simply reduce the thickness of the DKC coating below the critical cracking thickness because the largest pore size was evaluated by the bubble point method, which indicates the size of the pore-throat in the pore channel [35]. Therefore, if the ratio of kaolin in a DKC coating is locally inhomogeneous, the largest pore size will not be effectively reduced even after deposition of the coating. Even if only a certain area of the coating has a relatively large 'largest pore size' due to an insufficient amount of kaolin, then this figure will be taken as the largest pore size of the entire area. Thus, to guarantee an effective decrease in the largest pore size when using irregular and porous diatomite particles, the DKC coating should be as thick as possible.

Micro-cracks may also be generated during the sintering process. Prior to depositing the DKC coating onto the DS layer, the linear shrinkage of both bulk diatomite and kaolin were measured. After dry-pressing at 25 MPa and then sintering at 1200 °C for 1 h, the linear shrinkage rates of diatomite and kaolin were 2.47% and 11.19%, respectively. Therefore, as the amount of kaolin added to the coating increased, the difference between the linear shrinkage of the DKC coating and the DS layer increased. Moreover, the DS layer was sintered before the coating process started, leaving it very little shrinking potential to match the shrinkage of the DKC coating when they were later sintered together.

To reduce the generation of micro-cracks during the drying and sintering processes and to investigate the effect of the aforementioned linear shrinkage difference between the DKC coating and the DS layer, we designed two experiments. The goal of the first experiment was to create a diatomite–kaolin composite intermediate (DKCI) layer with a diatomite coating. In the second experiment, the goal was the reverse: to create a diatomite intermediate (DI) layer with a DKC coating.

First, a DKCI layer was coated over a DS layer and covered by a diatomite coating (Diatomite membrane type III, as shown in Fig. 1e). This combination could not exclude the possibility of micro-crack generation due to the shrinkage difference between the DKCI and DS layers; however, it was worth investigating whether a diatomite coating could act as a healing layer for an area with micro-cracks in the DKCI layer. As shown in Fig. 2b, the micro-cracks and voids in Fig. 3a

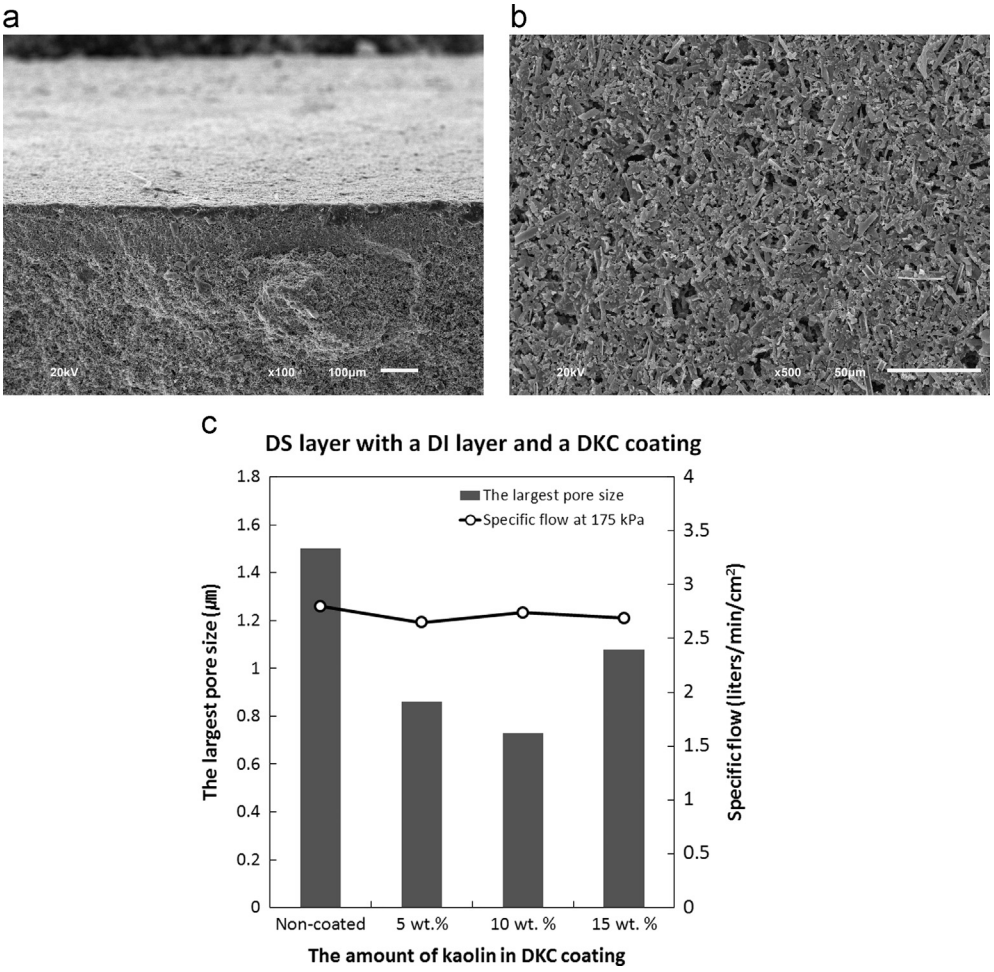

Fig. 4. (a) Cross-sectional SEM image of the diatomite–kaolin composite coating prepared with 10 wt% kaolin deposited over a diatomite intermediate layer on a diatomite support layer and sintered at 1200 °C for 1 h, (b) surface SEM image of a diatomite–kaolin composite coating, and (c) the permeability and largest pore size of the diatomite–kaolin composite coating deposited over a diatomite intermediate layer on the diatomite support layer.

occur between a DKCI layer and a DS layer. In addition, Fig. 3b demonstrates that the largest pore size of the diatomite membrane was reduced only when the amount of added kaolin was small. The effect of incorporating a DKCI layer decreased gradually as the amount of kaolin increased. The data for the largest pore size show that the micro-cracks generated between the DKCI and DS layers, even with increasing amounts of kaolin, could not be fully covered or filled by a diatomite coating. Accordingly, we determined that the largest pore size could only be reduced effectively by suppressing the generation of micro-cracks, not by covering or filling them.

Second, to prevent the generation of micro-cracks, we created a diatomite intermediate (DI) layer between a DKC coating and a DS layer (Diatomite membrane type IV, as shown in Fig. 1e). We considered that the difference in shrinkage might be reduced if the sintered DS layer faced a dried diatomite coating, instead of a dried DKC coating.

Cross-sectional (Fig. 4a) and surface (Fig. 4b) SEM images show a DKC coating prepared with 10 wt% kaolin over a DKCI layer coated onto the DS layer and then sintered at 1200 °C for 1 h. Indications of defects or delamination among the DKC coating, the DKCI layer, and the DS layer were not observed in the cross-sectional SEM images. In addition, the surface SEM image clearly shows that there were no micro-cracks on the DKC coating except for the original voids in the diatomite matrix. Fig. 4c supports the overall absence of micro-cracks in the coating by showing that the largest pore size significantly decreased while the permeability of the DS layer was retained as expected. With 15 wt% kaolin in the DKC coating, the largest pore size increased again due to defects induced by the drying and sintering processes. In addition, even with a diatomite intermediate layer, micro-cracks in the DKC coating were observed when the amount of kaolin added exceeded 10 wt%.

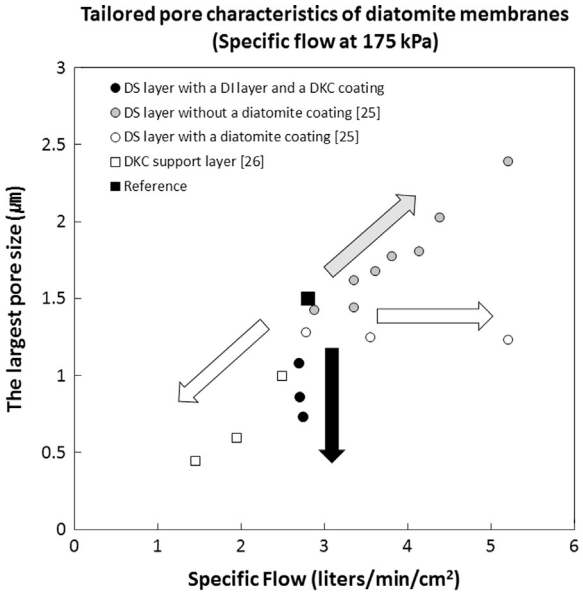

Fig. 5. Largest pore sizes of diatomite membranes created under various processing conditions as a function of the specific flow rate at 175 kPa.

In summary, Fig. 5 shows that we could design the pore characteristics of a diatomite membrane as desired. The permeability of a diatomite membrane could be enhanced by a sacrificial template method at the expense of increasing the largest pore size [27] (the direction of the dark-grey arrow). By adopting the diatomite coating, the increase in the largest pore size could be suppressed [27] (the direction of the white arrow). To decrease the largest pore size of a diatomite membrane while not changing its permeability, a diatomite intermediate layer was deposited on a DS layer, then covered with a DKC coating (the direction of the black arrow). If the largest pore size of a diatomite membrane needs to be reduced further at the expense of the permeability, the addition of kaolin directly to a DS layer would be one way to do so [28] (the direction of the light-grey arrow).

4. Conclusion

In summary, we prepared a diatomite membrane with a diatomite–kaolin composite coating layer. This composite coating was thick enough to reduce the largest pore size effectively and thin enough not to deteriorate the permeability to an unacceptable level. Moreover, by adopting a diatomite intermediate layer, a diatomite membrane with a composite coating that lacked the micro-cracks that tend to be induced by the drying and sintering processes was prepared.

It is noteworthy that the largest pore size of the diatomite membrane could be reduced while retaining an acceptable level of permeability by adding kaolin not to a support layer but to a surface layer (coating), which provided an effective means of tailoring the pore characteristics of the resultant membrane matrix. Furthermore, the largest pore sizes of the diatomite membranes could be controlled within the sub-micron size range. These findings demonstrate the feasibility of using a modified diatomite membrane as a porous ceramic membrane for microfiltration.

Acknowledgments

This study was supported financially by Fundamental Research Program of the Korean Institute of Materials Science (KIMS).

References

[1] A.R. Studart, U.T. Gonzenbach, E. Tervoort, L.J. Gauckler, Processing routes to macroporous ceramics: a review, Journal of the American Ceramic Society 89 (2006) 1771–1789.
[2] N. van Garderen, F.J. Clemens, M. Mezzomo, C.P. Bergmann, T. Graule, Investigation of clay content and sintering temperature on attrition resistance of highly porous diatomite based material, Applied Clay Science 52 (2011) 115–121.
[3] U.T. Gonzenbach, A.R. Studart, D. Steinlin, E. Tervoort, L.J. Gauckler, Processing of particle-stabilized wet foams into porous ceramics, Journal of the American Ceramic Society 90 (2007) 3407–3414.
[4] Z.-Y. Deng, J.M.F. Ferreira, Y. Tanaka, Y. Isoda, Microstructure and thermal conductivity of porous ZrO2 ceramics, Acta Materialia 55 (2007) 3663–3669.

[5] F. Raether, M. Iuga, Effect of particle shape and arrangement on thermoelastic properties of porous ceramics, Journal of the European Ceramic Society 26 (2006) 2653–2667.
[6] B. Nait-Ali, K. Haberko, H. Vesteghem, J. Absi, D.S. Smith, Thermal conductivity of highly porous zirconia, Journal of the European Ceramic Society 26 (2006) 3567–3574.
[7] Z. Hou, F. Ye, L. Liu, Q. Liu, H. Zhang, Effects of solid content on the phase assemblages, mechanical and dielectric properties of porous α-SiAlON ceramics fabricated by freeze casting, Ceramics International 39 (2013) 1075–1079.
[8] C.-H. Chen, K. Takita, S. Ishiguro, S. Honda, H. Awaji, Fabrication on porous alumina tube by centrifugal molding, Journal of the European Ceramic Society 25 (2005) 3257–3264.
[9] M. Wegmann, B. Michen, T. Graule, Nanostructured surface modification of microporous ceramics for efficient virus filtration, Journal of the European Ceramic Society 28 (2008) 1603–1612.
[10] H. Qi, S. Niu, X. Jiang, N. Xu, Enhanced performance of a macroporous ceramic support for nanofiltration by using α-Al2O3 with narrow size distribution, Ceramics International 39 (2013) 2463–2471.
[11] S.S. Madaeni, H. Ahmadi Monfared, V. Vatanpour, A. Arabi Shamsabadi, E. Salehi, P. Daraei, S. Laki, S.M. Khatami, Coke removal from petrochemical oily wastewater using γ-Al2O3 based ceramic microfiltration membrane, Desalination 293 (2012) 87–93.
[12] B.K. Nandi, R. Uppaluri, M.K. Purkait, Preparation and characterization of low cost ceramic membranes for micro-filtration applications, Applied Clay Science 42 (2008) 102–110.
[13] L. Kang, Ceramic Membranes for Separation and Reaction, John Wiley & Sons, Ltd., London, 2007.
[14] N. van Garderen, F.J. Clemens, J. Kaufmann, M. Urbanek, M. Binkowski, T. Graule, C.G. Aneziris, Pore analyses of highly porous diatomite and clay based materials for fluidized bed reactors, Microporous and Mesoporous Materials 151 (2012) 255–263.
[15] H. Giesche, Mercury porosimetry: a general (practical) overview, Particle and Particle Systems Characterization 23 (2006) 9–19.
[16] A.L. Ahmad, C.P. Leo, S.R. Abd. Shukor, Tailoring of a γ-alumina membrane with a bimodal pore size distribution for improved permeability, Journal of the American Ceramic Society 91 (2008) 246–251.
[17] A. Pruchnewski, Effect of sintering temperature on functional properties of alumina membranes, Journal of the European Ceramic Society 22 (2002) 613–623.
[18] A.L. Ahmad, M.A.T. Jaya, C.J.C. Derek, M.A. Ahmad, Synthesis and characterization of TiO2 membrane with palladium impregnation for hydrogen separation, Journal of Membrane Science 366 (2011) 166–175.
[19] E. Chevereau, N. Zouaoui, L. Limousy, P. Dutournié, S. Déon, P. Bourseau, Surface properties of ceramic ultrafiltration TiO_2 membranes: effects of surface equilibriums on salt retention, Desalination 255 (2010) 1–8.
[20] C.C. Coterillo, T. Yokoo, T. Yoshioka, T. Tsuru, M. Asaeda, Synthesis and characterization of microporous ZrO_2 membranes for gas permeation at 200 °C, Separation Science and Technology 46 (2011) 1224–1230.
[21] G.T. Lim, H.G. Jeong, I.S. Hwang, D.H. Kim, N. Park, J. Cho, Fabrication of a silica ceramic membrane using the aerosol flame deposition method for pretreatment focusing on particle control during desalination, Desalination 238 (2009) 53–59.
[22] J. Kim, B. Van der Bruggen, The use of nanoparticles in polymeric and ceramic membrane structures: review of manufacturing procedures and performance improvement for water treatment, Environmental Pollution 158 (2010) 2335–2349.
[23] A. Cheraitia, A. Ayral, A. Julbe, V. Rouessac, H. Satha, Synthesis and characterization of microporous silica-alumina membranes, Journal of Porous Materials 17 (2010) 259–263.
[24] D. Losic, J.G. Mitchell, N.H. Voelcker, Diatomaceous Lessons in nanotechnology and advanced materials, Advanced Materials 21 (2009) 2947–2958.
[25] B. Michen, F. Meder, A. Rust, J. Fritsch, C. Aneziris, T. Graule, Virus removal in ceramic depth filters based on diatomaceous earth, Environmental Science and Technology 46 (2012) 1170–1177.
[26] F. Akhtar, Y. Rehman, L. Bergström, A study of the sintering of diatomaceous earth to produce porous ceramic monoliths with bimodal porosity and high strength, Powder Technology 201 (2010) 253–257.
[27] J.-H. Ha, E. Oh, I.-H. Song, The fabrication and characterization of sintered diatomite for potential microfiltration applications, Ceramics International (2013) http://dx.doi.org/10.1016/j.ceramint.2013.02.102.
[28] J.-H. Ha, E. Oh, B. Bae, I.-H. Song, The effect of kaolin addition on the characteristics of a sintered diatomite composite support layer for potential microfiltration applications. Ceramics International, http://dx.doi.org/10.1016/j.ceramint.2013.04.092, in press.
[29] H.H. Murray, Traditional and new applications for kaolin, smectite, and palygorskite: a general overview, Applied Clay Science 17 (2000) 207–221.
[30] R.D. Deegan, O. Bakajin, T.F. Dupont, G. Huber, S.R. Nagel, T.A. Witten, Capillary flow as the cause of ring stains from dried liquid drops, Nature 389 (1997) 827–829.
[31] H.-J. Son, R.-H. Song, T.-H. Lim, S.-B. Lee, S.-H. Kim, D.-R. Shin, Effect of fabrication parameters on coating properties of tubular solid oxide fuel cell electrolyte prepared by vacuum slurry coating, Journal of Power Sources 195 (2010) 1779–1785.
[32] K.B. Singh, M.S. Tirumkudulu, Cracking in drying colloidal films, Physical Review Letters 98 (2007) 218302.
[33] R.C. Chiu, T.J. Garino, M.J. Cima, Drying of granular ceramic films: I. Effect of processing variables on cracking behavior, Journal of the American Ceramic Society 76 (1993) 2257–2264.
[34] R.C. Chiu, M.J. Cima, Drying of granular ceramic films: II. drying stress and saturation uniformity, Journal of the American Ceramic Society 76 (1993) 2769–2777.
[35] J. Yu, X. Hu, Y. Huang, A modification of the bubble-point method to determine the pore-mouth size distribution of porous materials, Separation and Purification Technology 70 (2010) 314–319.